PASSIVE AND ACTIVE NEAR-SURFACE MOUNTED FRP RODS FOR FLEXURAL STRENGTHENING OF RC BEAMS

Laura De Lorenzis, University of Lecce, Lecce, ITALY
Francesco Micelli, University of Lecce, Lecce, ITALY
Antonio La Tegola, University of Lecce, Lecce, ITALY

Abstract

Among the strengthening techniques based on Fiber Reinforced Polymer (FRP) composites, the use of near-surface mounted (NSM) FRP rods is emerging as a promising technology for increasing flexural and shear strength of deficient concrete, masonry and timber members. In this project, flexural strengthening was investigated by testing six 4.3-m long reinforced concrete (RC) beams with 200x400 mm rectangular cross-section. Carbon FRP rods were embedded in grooves cut onto the bottom concrete surface and filled with a two-component, viscous epoxy paste. The investigated variables were the ratio of internal steel reinforcement and the ratio of FRP superficial reinforcement. All the beams were loaded under four-point bending and instrumented with LVDTs and strain gages to monitor deflection and strains at various locations on concrete and FRP. Further tests are already ongoing in which the type of strengthening is active rather than passive. Active strengthening can be achieved by prestressing the NSM FRP rod by means of mechanical tensioning and anchoring devices. Such devices have been designed and are also presented in the paper. They allow to strengthen an RC beam with active NSM FRP rods in a real situation, when typically no access to the beam ends is allowed by the boundary conditions.

Introduction

The use of Near Surface Mounted (NSM) Fiber Reinforced Polymer (FRP) rods is an attractive method for increasing flexural and shear strength of deficient reinforced concrete (RC) members and masonry walls and, in certain cases, can be more convenient than using FRP laminates. Application of NSM FRP rods does not require surface preparation work (other than grooving) and implies minimal installation time compared to FRP laminates. The use of customized grooving tools can allow technicians to cut the appropriate grooves in one pass, whereas the choice of high-viscosity epoxies as groove-filling material allows to easily gun the material in the groove even when strengthening members for positive moments. Another advantage is the feasibility of anchoring these rods into members adjacent to the one to be strengthened. This technique becomes particularly attractive for strengthening in the negative moment regions of slabs and decks, where external reinforcement would be subjected to mechanical and environmental damage and would require protective cover which could interfere with the presence of floor finishes. Finally, NSM rods offer better fire performance compared to externally bonded laminates due to the protection of the encapsulating material.

Limited literature is available to date on the use of NSM FRP rods for flexural strengthening of RC beams. Tests have been conducted by Crasto et al. [1], De Lorenzis et al. [2] and Rizkalla and Hassan [3]. Once the technology emerges, a larger experimental database is needed to confirm and quantitatively evaluate its effectiveness. It is of interest to verify to what extent the usual design approach based on the traditional RC theory is able to accurately predict behavior and capacity of RC beams strengthened in bending with NSM FRP rods. As the critical failure mechanisms may include debonding of the external reinforcement, specific design equations are needed that must be validated through comparison with experimental results.

In this project, flexural strengthening was investigated by testing six RC beams with rectangular cross-section. Carbon FRP rods were embedded in grooves cut onto the bottom concrete surface and filled with a two-component, viscous epoxy paste. The investigated variables were the ratio of internal steel reinforcement and the ratio of FRP superficial reinforcement.

Further tests are already ongoing in which the type of strengthening is active rather than passive. The use of post-tensioned FRP reinforcement should result very effective as it should allow to achieve advantages at both the serviceability and the ultimate limit states. Active strengthening can be achieved by prestressing the NSM FRP rod by means of mechanical tensioning and anchoring devices. Such devices have been designed and are also presented as follows. Their configuration allows to strengthen an RC beam with prestressed NSM FRP rods in a real situation, when typically no access to the beam ends is allowed by the boundary conditions.

Experimental Tests

Specimens

Six RC beams with 200x400 mm rectangular cross-section and a total length of 4.3-m were tested. All the beams had internal steel flexural and shear reinforcement, designed according to the specifications of the ACI Building Code [4]. The flexural reinforcement on the tension side consisted of two 14-mm steel rebars for three beams (a-series) and of two 18-mm steel rebars for the other three beams (b-series). The corresponding longitudinal tension reinforcement ratios were both greater than the ACI minimum and approximately equal to 46% and 80% of the ACI maximum (that is, they were approximately 35% and 59% of the balanced amount), respectively. All beams had two 12-mm steel rebars on the compression side. The shear reinforcement, designed to ensure that flexural failure would control, consisted of 8-mm steel stirrups spaced 200 mm o.c. Table 1 summarizes the tested beams, and a detail of the beams cross-section is illustrated in Figure 1. Beams BC-a and BC-b (with no external strengthening) were used as a baseline comparison to evaluate the enhancement in strength provided by the NSM FRP rods. Beams BR1-a and BR1-b were strengthened with one 8-mm CFRP rods. The corresponding theoretical failure mode was concrete crushing after steel yielding, with imminent FRP rupture only for BR1-a. Beams BR2-a and BR2-b were strengthened with two 8-mm CFRP rods and their theoretical failure mode was concrete crushing after steel yielding.

The grooves were saw cut with a concrete saw upon hardening of the beams. All grooves had square cross-section, with size of 16 mm, corresponding to a groove-size-to-bar-diameter ratio equal to 2.0. The NSM rods were prolonged above the supports until the beam ends, to simulate a real situation with anchorage of the rods into the adjacent structural members.

Materials

The target concrete strength required from the ready-mix supplier was 30 MPa. Due to a mistake in the concrete mix, the actual average concrete strength, determined according to ASTM C39-97 on three 150-mm diameter by 300-mm concrete cylinders, was only equal to 15 MPa. The nominal yield strength of the steel tension and compression reinforcement was 435 MPa. The actual yield strengths of the 14-mm and 18-mm tension reinforcement, as determined from tensile test on three coupon specimens according to ASTM A370-97, were 496 MPa and 510 MPa, respectively.

A commercially available epoxy paste was used for embedding the rods. Its mechanical properties as specified by the manufacturer were: 30 MPa bending tensile strength, 80 MPa compressive strength, 6265 MPa secant modulus in compression. CFRP spirally-wound and sand-coated bars with 8-mm diameter were the NSM reinforcement. Their mechanical properties were: 2400 MPa tensile strength and 128.8 GPa Young's modulus [5].

Table 1. Summary of Specimens and Results

Beam	Flex. Reinf. (Tension)	FRP Reinf.	Experimental		Theoretical		% Error	% Increase over BC (Exp.)
			Ultimate Load (kN)	Failure Mode	Ultimate Load (kN)	Failure Mode		
BC-a	2 ϕ14	-	60.6	CC after SY	60.7	CC after SY	0.2	-
BC-b	2 ϕ18	-	103.1	CC after SY	100.4	CC after SY	-2.6	-
BR1-a	2 ϕ14	1 ϕ 8	84.7	DB after SY	95.4	CC after SY	12.6	39.8
BR1-b	2 ϕ18	1 ϕ 8	125.1	CC after SY	121.7	CC after SY	-2.7	21.3
BR2-a	2 ϕ14	2 ϕ 8	97.3	DB after SY	113.5	CC after SY	16.7	60.6
BR2-b	2 ϕ18	2 ϕ 8	135.4	CC after SY - DB	134.2	CC after SY	-0.9	31.3

CC = Concrete Crushing; DB = Debonding; SY = Steel Yielding

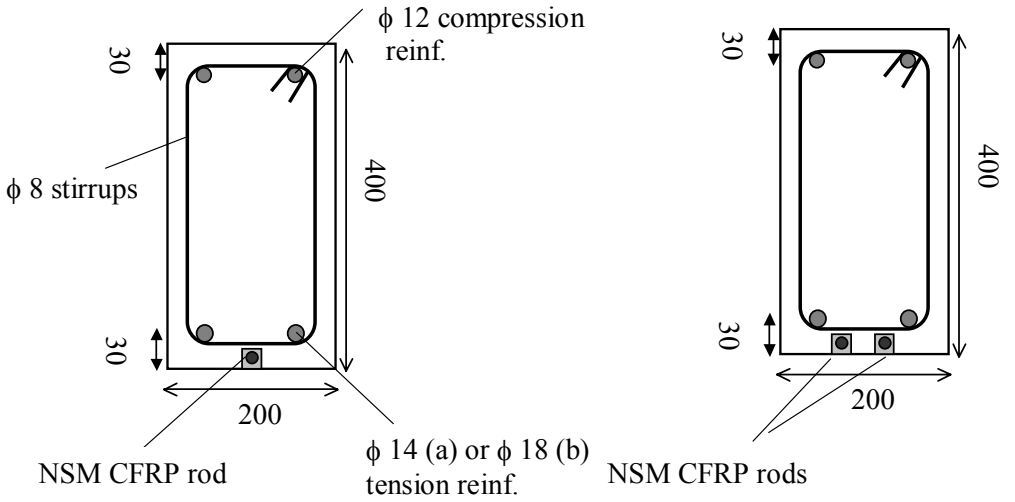

Figure 1. Cross-Section of the Beams

Procedure and Instrumentation

The epoxy paste was allowed to cure for 15 days at room temperature prior to testing. The beams were loaded under four-point bending with a net span of 4.0 m and a shear span of 1.75 m. Load was applied by means of a 200-ton hydraulic jack connected to an electric pump and recorded with a 200-ton. load cell.

Each beam was instrumented with four LVDTs placed at mid-span on both sides and at both quarter-spans on one side. Dial gages were also placed at each support to derive the net deflections. Strain gages were applied on concrete and FRP rods at various locations. Figure 2 is a picture of the test setup.

Section Analysis

For the theoretical analysis of the cross-section, several assumptions commonly made in reinforced concrete theory were used:

1) plane cross-sections remain plane;
2) small deformations;
3) no slip between any longitudinal reinforcement and concrete;
4) no tensile strength of concrete after cracking;
5) stress-strain relationships of materials as determined by standard uniaxial tests are representative of their behavior as part of the beam.

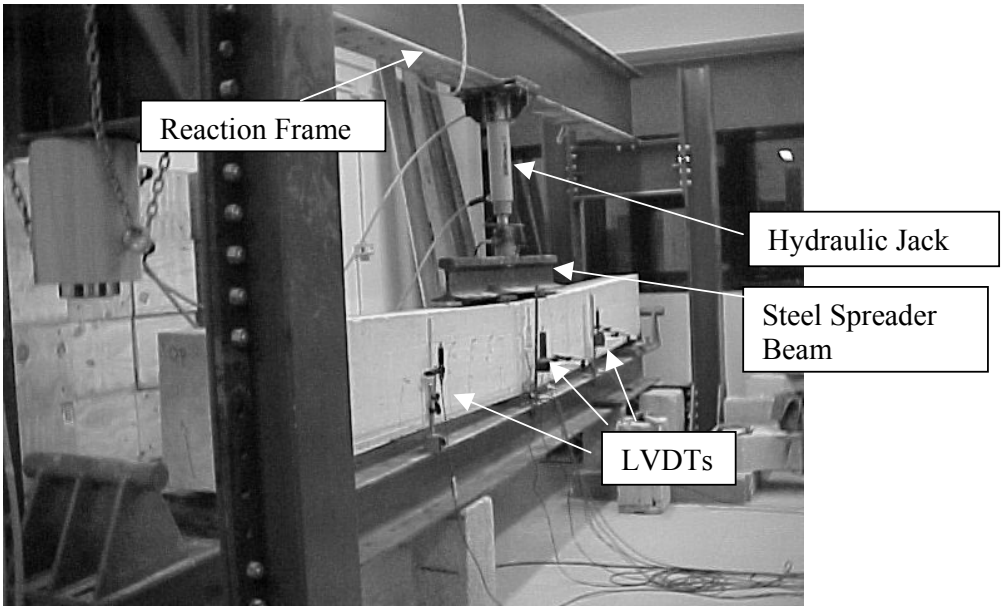

Figure 2. Test Setup

The stress-strain relationship for the steel rebars in tension was obtained experimentally. An elastic-plastic behavior followed by a strain hardening branch was observed. The hardening branch was neglected in modeling and an idealized elastic – perfectly plastic behavior was assumed. The steel rebars in compression and the FRP rods were modeled as elastic-perfectly plastic and linearly elastic up to failure, respectively. A parabolic stress-strain curve was adopted for concrete in uniaxial compression:

$$f_c = f'_c \left[\frac{2\varepsilon_c}{\varepsilon'_c} - \left(\frac{\varepsilon_c}{\varepsilon'_c} \right)^2 \right] \quad (1)$$

where f'_c is the concrete compressive strength, ε_c and f_c are the concrete compressive strain and stress, respectively, and ε'_c is the strain corresponding to the maximum stress, which was assumed equal to 0.002.

The cracking moment and curvature were computed by elastic analysis of the homogeneized cross-section. The moment-curvature diagram after cracking was generated for each beam by increasing the strain in the concrete top fiber, $\overline{\varepsilon_c}$, in specified increments until failure. For each value of $\overline{\varepsilon_c}$, the neutral axis depth was calculated by using compatibility of strains and equilibrium of forces; stresses in tension steel, compression steel and FRP rods and curvature of the cross-section were computed; finally, the internal moment was calculated by equilibrium of moments. It was assumed that failure occurred when either the concrete strain reached 0.003 or the FRP rebars attained their ultimate strain. The moment-curvature points were plotted and the resulting curve was simplified as having three linear branches: 1) before cracking, 2) after cracking and before yielding of the longitudinal tension steel, 3) after yielding of the longitudinal tension steel up to failure. Finally, the load-deflection curve was obtained using a cross-sectional approach, that is, doubly integrating the simplified moment-curvature relationship over the length of the beam.

Results

A summary of experimental and theoretical results is reported in Table 1. Beams BC-a and BC-b, with no external strengthening, failed at a load of 60.6 and 103.1 kN, respectively, by concrete crushing after yielding of the steel tension reinforcement. Ultimate load and failure mode were in

close agreement with the prediction of the analytical model. The experimental and theoretical load-deflection curves are reported in Figure 3, showing good correlation up to the ultimate load.

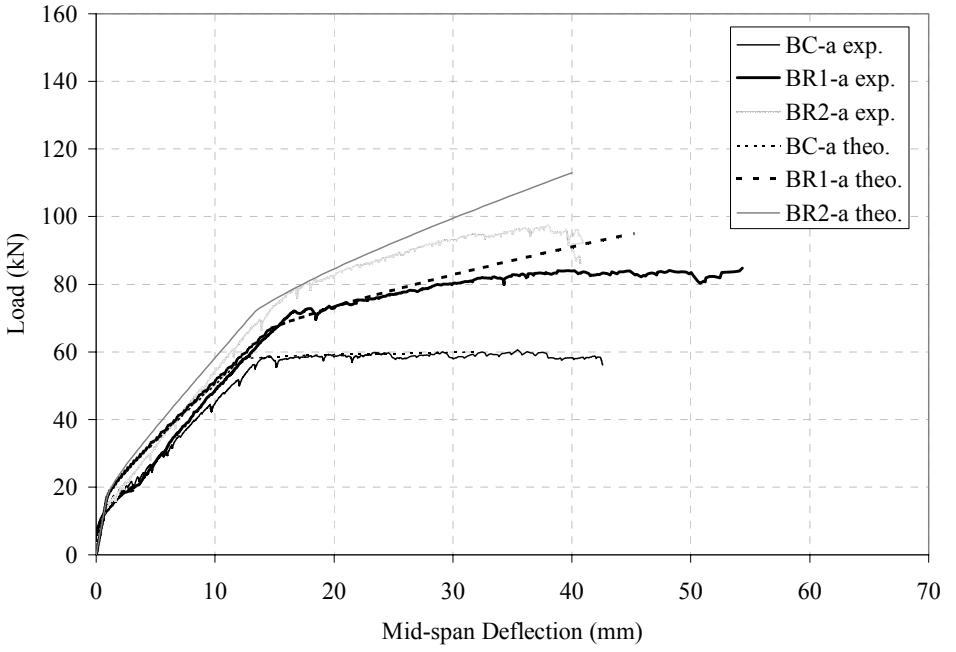

(a)

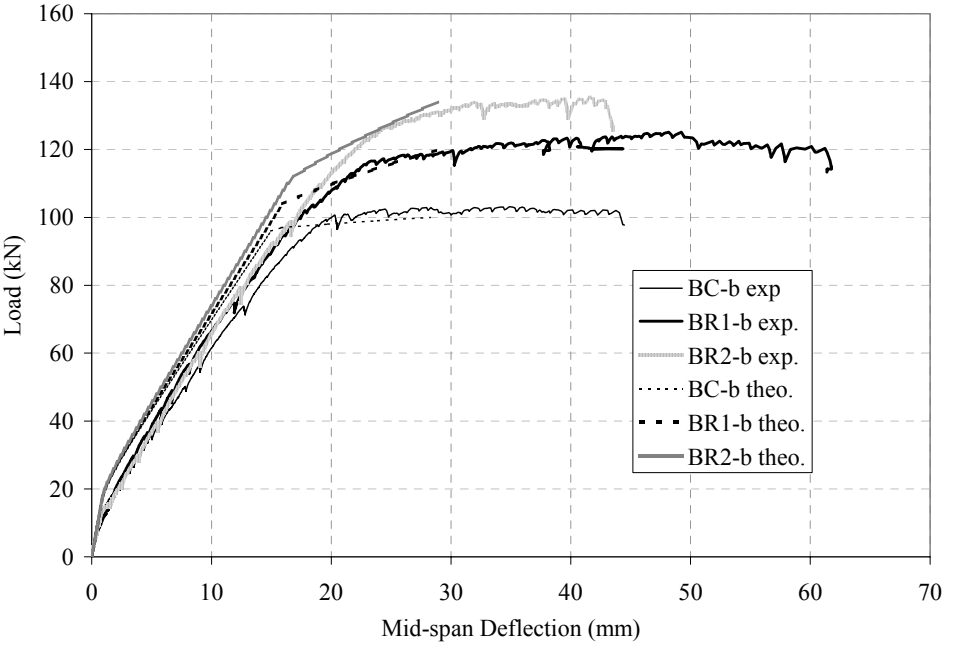

(b)

Figure 3. Experimental and Theoretical Load vs. Mid-span Deflection Curves of the Tested Beams: a-series (a) and b-series (b).

Also reported in the same figures are the load-deflection curves of the strengthened beams. The global behavior was common to all beams. As a result of the external strengthening, a moderate increase in stiffness was achieved in the region between cracking of the concrete and yielding of the steel longitudinal reinforcement. Also, the yielding load, corresponding to the change in slope of the curve, increased appreciably. After yielding, the control beams had a flat load-deflection behavior,

whereas in the strengthened beams yielding of the steel rebars led to a reduction in slope, but the FRP rod allowed the beam to take additional load. Theoretical and experimental curves generally correlate well up to yielding. In the post-yielding phase, the stiffness of the experimental load-deflection curve was usually lower than predicted, due to slippage of both steel and NSM reinforcement. Prediction of the ultimate load was very accurate when failure was by concrete crushing after yielding of the steel reinforcement; less accurate (with errors varying from 13% to 17%) when failure occurred by debonding mechanisms, not accounted for in the model.

Also common to all strengthened beams was the general cracking behavior: after first cracking, the number of cracks gradually increased until the stabilized cracking pattern was reached. At this point, the existing cracks started to increase in size up to yielding of the steel reinforcement. After yielding, the primary cracks "bifurcated" at the level of the steel bars generating many closely spaced secondary cracks, some of which tended to propagate horizontally along the concrete cover. Evolution of this crack pattern, and hence the final failure mode, depended on the steel and FRP reinforcement ratio of the beams.

Failure of Beam BR1-a, strengthened with one NSM CFRP rod, occurred under an applied load of 84.7 kN, corresponding to a 39.8% increase in capacity with respect to the control beam BC-a. The failure mode was debonding of the NSM rod. A typical crackling noise during the test revealed the progressive internal micro-cracking of the epoxy paste, especially in the post-yield phase when the increase in load was almost entirely taken by the NSM rod and its tensile stress increased considerably. Inclined and longitudinal cracks formed in the concrete surrounding the epoxy-filled groove. Such "bond" cracks were mainly located near each flexural crack and at the ends of the beam, that is, at the locations where bond stresses are maximum due to the transfer of stresses between the concrete and the NSM reinforcement. Finally, part of the concrete cover of the internal steel reinforcement was split off in a catastrophic fashion starting from the maximum moment region (Figure 4-a) and the epoxy prisms detached from the concrete with a thin layer of concrete remaining attached to their surface (Figure 4-b). After failure, the load dropped to a value close to the capacity of the control beam and deflection kept on increasing, until the test was stopped. This part of the load-deflection curve has not been reported. Due to "premature" bond failure, the experimental ultimate load was about 13% lower than the theoretical one.

Beam BR1-b failed at 125.1 kN, which indicated a 21.3% increase over BC-b. The load-deflection behavior of the beam was as described for BR1-a, and is reported in Figure 3. In this case, due to the higher steel reinforcement ratio, the failure mode was concrete crushing after yielding of the steel longitudinal tension reinforcement. However, also in this beam inclined and longitudinal bond cracks formed in the concrete surrounding the epoxy and were visible after failure.

Failure of Beam BR2-a occurred under an applied load of 97.3 kN, corresponding to a 60.6% increase in capacity with respect to the control beam BC-a and to a 14.9% increase over BR1-a. The higher FRP reinforcement ratio should have made debonding less critical for this beam than for BR1-b. However, the presence of two NSM bars side by side at relatively close distance between each other and with the edges (30-mm clear distance between the grooves, equal to about 1.8 times the groove size; 69-mm clear distance from the edge, equal to about 4.3 times the groove size) generated higher stresses in the concrete surrounding the grooves, similarly to what happens in lap splices of steel reinforcement in concrete. The failure mode was debonding of the NSM rods by spalling of the concrete cover of the longitudinal reinforcement along the edges of the beam (Figure 5). This suggests that, when using more than one NSM bar for strengthening, the distance between two adjacent grooves and the distance of each groove from the edges of the beam should not be less than a minimum value to be established upon appropriate testing.

(a)

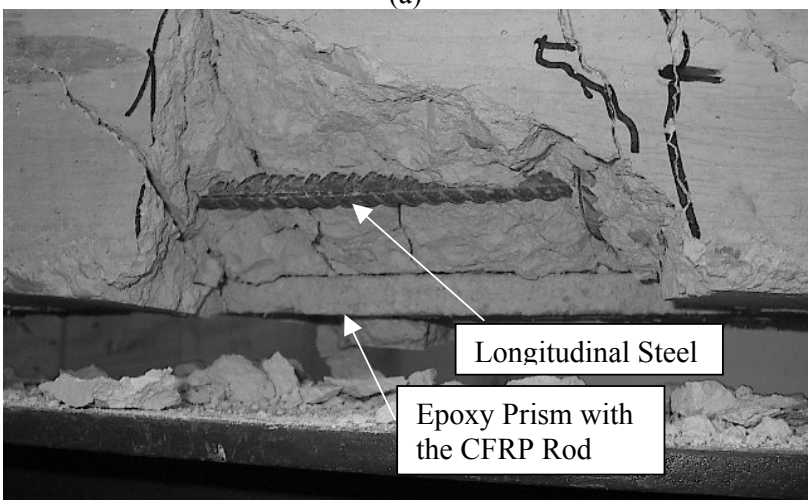

(b)

Figure 4. Failure of Beam BR1-a

Beam BR2-b failed at a load of 135.4 kN, corresponding to a 31.3% increase in capacity with respect to BC-b but only to 8.2% increase over BR1-b. The failure mode was again concrete crushing after yielding of the steel tension reinforcement. Despite the FRP tensile stress at failure was lower than in beam BR1-b due to the higher reinforcement ratio, the presence of two NSM bars gave rise to a higher stress state in the concrete surrounding the grooves, as noted for beam BR2-a. As a result, immediately after concrete crushing, the two epoxy prisms in which the CFRP bars were embedded (along with the concrete in between) and part of the concrete cover of the internal steel reinforcement were split off as described for beam BR1-a.

Figures 6 and 7 show the theoretical and experimental load vs. FRP and top concrete strain at mid-span. After steel yielding, the strain in the FRP increased at a much faster rate as indicated by the reduced slope of the curve. This is due to the fact that, after the rebars yielded, the FRP alone resisted further increments of the tensile component of the internal moment couple. There is good agreement between experimental and theoretical results up to the experimental ultimate load.

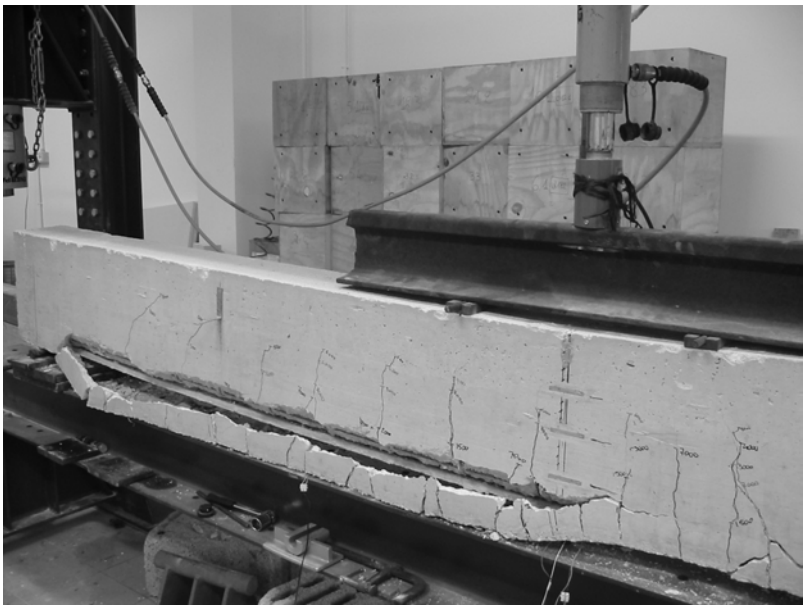

Figure 5. Failure of Beam BR2-a

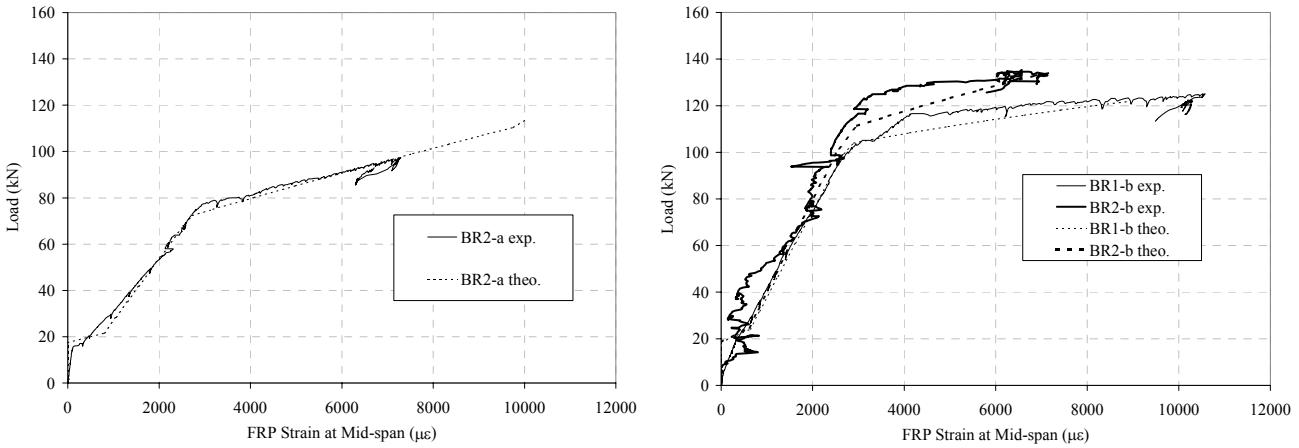

(a) (b)

Figure 6. Experimental and Theoretical Curves of Load vs. FRP Strain at Mid-span: a-series (a) and b-series (b).

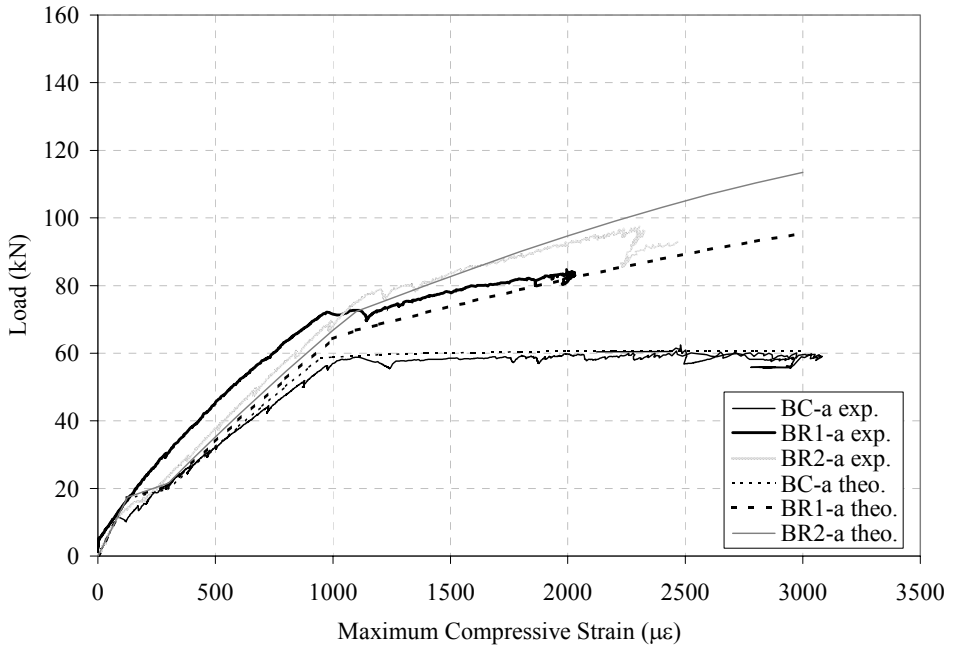

(a)

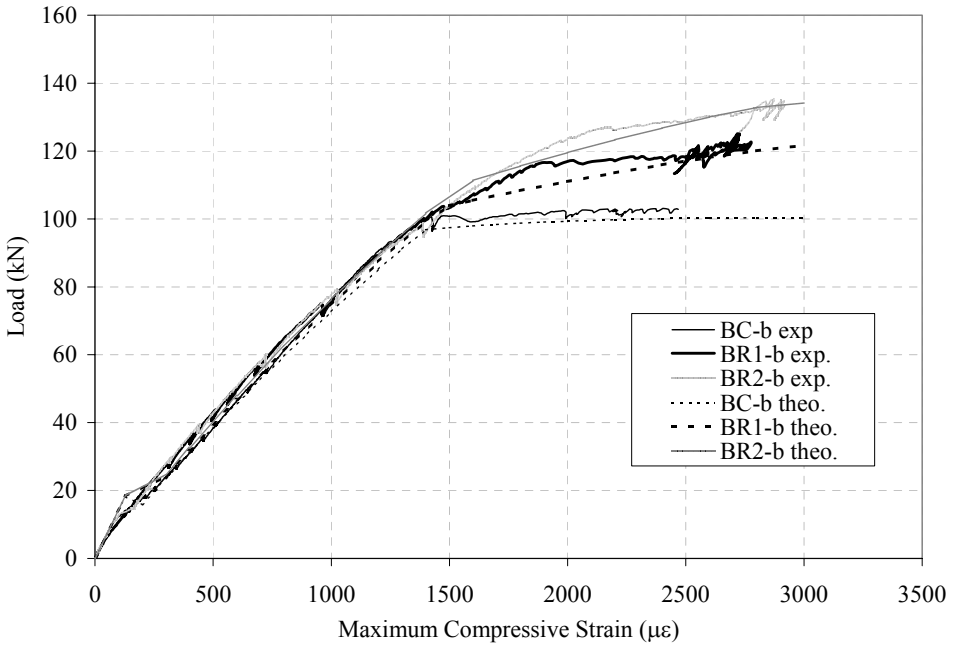

(b)

Figure 7. Experimental and Theoretical Curves of Load vs. Top Concrete Strain at Mid-span: a-series (a) and b-series (b).

Tensioning and Anchoring System for NSM FRP Rods

As visible from the load-deflection curves in Figure 3, strengthening with NSM FRP rods does not appreciably increase the stiffness of RC beams, but only their strength. In order for a stiffness increase to be achieved, the strengthening system must be active rather than passive, i.e., the NSM rods need to be prestressed or post-tensioned. In a real strengthening situation, there is no

access to the ends of the beam and therefore the traditional tensioning devices and anchoring plates cannot be used. Therefore, alternative solutions must be sought.

Figure 8 shows the proposed tensioning – anchoring device. The FRP rod in inserted into one side of a steel pipe and chemically bonded to it by an epoxy adhesive. The other end of the pipe is externally threaded. Another steel pipe is inserted on the first one and welded to one or more stainless steel anchors (substituted in the pictures by two steel reinforcing bars). The anchors are grouted into holes drilled in the concrete at the ends of the beam and the steel pipes are positioned into the groove (locally enlarged to contain them). Then, at one end of the beam the internal pipe is forced to move with respect to the external one (and hence the rod is forced to elongate) by tightening a nut on the internal pipe. An anti-torsional screw is used to prevent relative torsion of the two pipes during tightening and PTFE rings are inserted between the nut and the external pipe to reduce the bearing friction and facilitate manual tightening. This device is currently being used to strengthen two beams (identical to beams BR1-a and BR1-b) with active NSM rods.

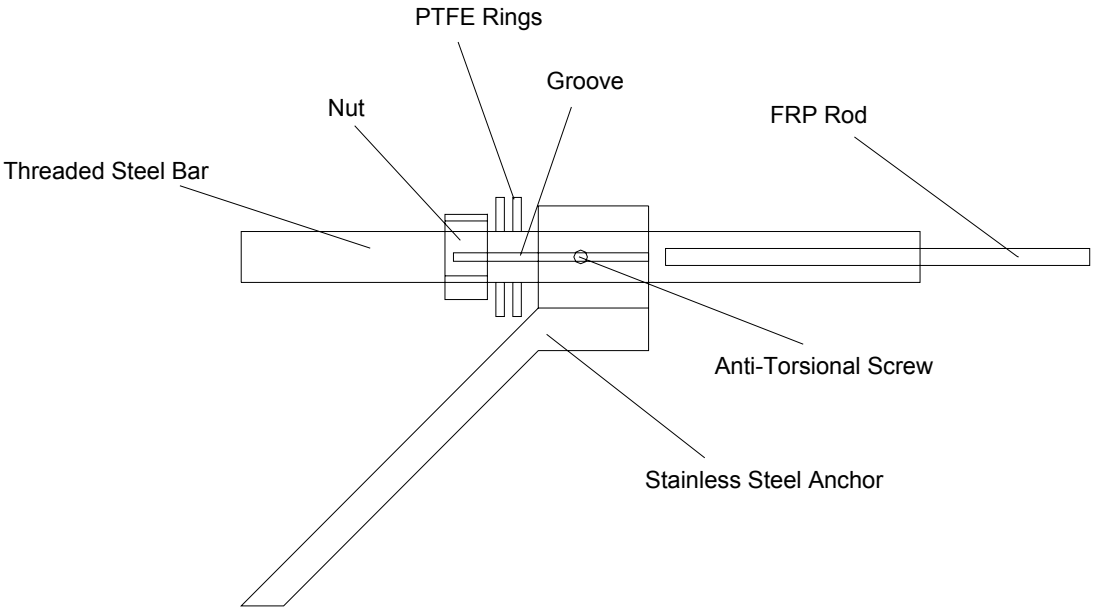

(a)

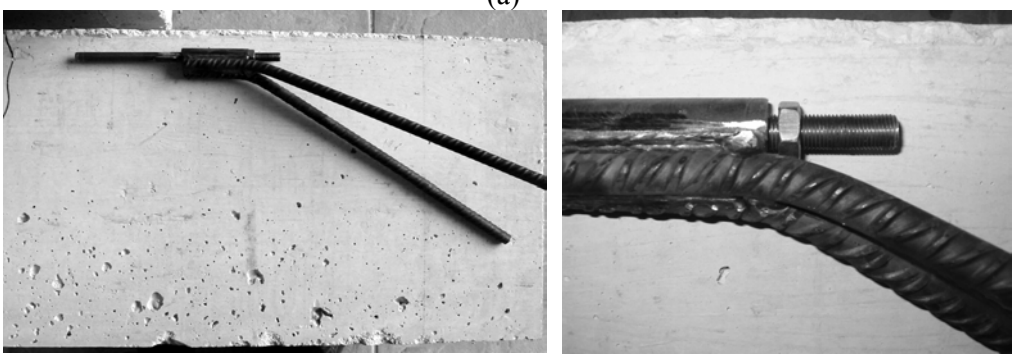

(b) (c)

Figure 8. Proposed Tensioning Device for NSM FRP Bars

Conclusions

Six full-size beams (two control and four strengthened beams) were tested, in which NSM CFRP rods were used for flexural strengthening. The test results confirm that NSM FRP rods can be used to significantly increase the flexural capacity of RC elements. In the tested beams, an increase

in the ultimate load ranging from 21.3% to 60.6% was achieved. The yielding load increased as well, whereas only moderate increases in stiffness were achieved. The failure mode was concrete crushing after yielding of the steel longitudinal reinforcement for the beams with the higher steel reinforcement ratio, and splitting of the concrete cover of the steel longitudinal reinforcement accompanied by debonding of the NSM rods for the other beams.

Results of the experimental tests were compared with the predictions of a simple model based on the traditional approach of reinforced concrete analysis. In most cases, a good agreement was observed between predicted and measured curves up to the yielding load. When failure was by concrete crushing, the ultimate load was very accurately predicted; in case of debonding failure, predictions were inaccurate on the unsafe side by 8.9% to 22.3%. However, even in case of "classical" crushing failure, the load-deflection behavior in the post-yielding phase was always less stiff than predicted, due to slip of steel and NSM reinforcement not accounted for in the cross-sectional approach.

As in the case of externally bonded laminates, bond may be the limiting factor on the efficiency of this technology, to an extent depending on a combination of different parameters: the internal steel reinforcement ratio, the FRP reinforcement ratio, the number of NSM bars, the surface configuration of the NSM bars, and obviously the concrete and epoxy tensile strength. While a general and detailed modeling of the debonding phenomenon including all these parameters is, at the present time, not feasible with the limited database available, results of this experimental tests along with those of previous investigations [2] gave clear qualitative indications on the effect of some of the aforementioned parameters.

A fundamental difference with respect to the case of externally bonded FRP laminates is that, when using NSM rods, they can be anchored into members adjacent to the strengthened one. Therefore, debonding is more critical in the maximum moment region. The nature of the debonding phenomenon depends on the surface configuration of the NSM bar.

When sandblasted bars are adopted, the bond strength at the bar-epoxy interface is rather limited and failure is most likely to occur by pull-out of the bar, consistently with what observed in the bond tests [2]. When deformed or spirally wound bars are used as NSM reinforcement, bond is mainly transferred by mechanical interlocking between bar and epoxy. If the grooves are saw-cut, i.e., if their surface is sufficiently rough to avoid bond failure at the epoxy-concrete interface, the weak links of the system become the concrete and the epoxy tensile strength. With a groove-size-to-bar-diameter-ratio equal to 2.0, such as in all tested beams, the controlling material has always been the concrete, even in the previous test series [2] where the epoxy tensile strength was rather low (about 14 MPa compared to 28 MPa of the epoxy in the present series). It is reasonable to expect that concrete with higher tensile strength offers more resistance to the development of the cracking pattern which leads to failure by debonding. Another relevant parameter in this context is the concrete fracture energy, which is regarded by current codes (e.g., [6]) as dependent on the concrete strength and maximum aggregate size. As beams of the current test series were made of very poor concrete (only 15-MPa compressive strength), their results can be considered conservative if extended to beams with normal-strength concrete.

Results of this and of the previous investigation indicate that debonding should be expected as critical failure mechanism when the FRP-strengthened cross-section is tension controlled, i.e. when, according to the traditional approach of RC theory, is predicted to fail by FRP rupture. All beams of the previous test series, designed to fail by FRP rupture, failed by debonding. When the strengthened cross-section is compression controlled, debonding is less critical, as the tensile stress in the FRP for a given value of top compressive strain is lower and so are the bond stresses. However, the chance of its occurrence increases as the FRP tensile stress at beam failure (as predicted by traditional RC theory) approaches the FRP tensile strength. Among beams of the present series, those with the highest steel reinforcement ratio (equal to 59% of the balanced amount) failed by concrete crushing, whereas the other two (with a steel reinforcement ratio equal to 35% of balanced) failed by debonding. It has also been noted that the presence of two NSM bars side by side

at relatively close distance (clear distance between the grooves and clear distance from the edge equal to about 1.8 times and 4.3 times the groove size, respectively) exerted an appreciable influence on the debonding crack pattern and load, as it generated "double" stresses in the concrete surrounding the grooves. This was indicated by the crack pattern at failure of beam BR2-a, but also confirmed by the behavior of beam BR2-b. As beam BR1-b had failed by concrete crushing, beam BR2-b should have *a fortiori* failed by the same mechanisms. It actually reached the predicted ultimate load associated by concrete crushing, but immediately afterwards it also displayed a "secondary" debonding failure.

Further research is needed to correlate the bond behavior of NSM rods observed in coupon-size specimens to debonding taking place in full-size beams and to the corresponding failure load.

Acknowledgements

The authors wish to acknowledge MAC Italia S.p.A. for supplying the materials used in this experimental program. This investigation was supported by the Italian Ministry of Research (MIUR) under program COFIN2000.

References

1. Crasto, A.; Kim, R.; and Ragland, W. (1999), Private Communication.
2. De Lorenzis, L., Nanni, A., La Tegola, A. (2000), "Flexural and Shear Strengthening of Reinforced Concrete Structures with Near Surface Mounted FRP Rods", Proceedings ACMBS III, Ottawa, Canada, August 15-18, pp. 521-528.
3. Rizkalla, S. and Hassan, T. (2001) "Various FRP Strengthening Techniques for Retrofitting Concrete Structures", *CICE 2001 Conference proceedings,* Hong Kong, December 2001.
4. American Concrete Institute (1999), Building Code Requirements for Structural Concrete (ACI 318-99) and Commentary (ACI 318R-99), ACI Committee 318, Detroit, MI.
5. Micelli, F., and Nanni, A., (2001), "Mechanical Properties and Durability of FRP Rods", CIES Technical Report 00-22, March 2001, 127 pp.
6. CEB-FIP Model Code 1990, CEB Bulletin d'Information No. 213/214, Lausanne 1993.